THE ASTROPHYSICAL JOURNAL, 287:307–314, 1984 December 1

THE SPACE ORIENTATION OF STARS

LAURANCE R. DOYLE[1]
3543 Santa Carlotta, La Crescenta, California
THOMAS J. WILCOX
Research and Development Laboratories
AND
JEAN J. LORRE
Research and Development Laboratories
Received 1984 January 20; accepted 1984 June 12

ABSTRACT

Stellar rotation periods recently determined from short-term variations in Ca II H and K emission-line flux associated with starspot activity can be combined with both rotational spectral line broadening velocity measurements and independent measurements of stellar radii to give the inclination of the star's rotation axis to the line of sight. Assuming that the limits of distribution of sunspots on the Sun apply similarly to solar-type stars, interferometric measurements of stellar radii in Ca II H and K flux may be performed to determine the clocklike, on-the-plane-of-the-sky orientation as well. Various stellar radius measuring techniques are discussed, and photon limits on the measurability of this latter parameter are derived for Ca II H and K speckle interferometry. The accuracy with which one can determine the space orientation of stars is discussed in the context of existing data as well as photon limits. The importance of determining the space orientation of stars is then discussed, with emphasis on its important application to the present search for extrasolar planetary systems.

Subject headings: Ca II emission — stars: rotation

I. INTRODUCTION

The space orientations of the rotation axes of single stars, with the exception of the Sun, have never been directly determined (Doyle, Wilcox, and Lorre 1983). However, spectroscopic variations with rotation period in Ap stars have allowed the determination of the inclination to the line-of-sight component for the rotation axes of these stars (see Abt 1972). In addition, close binaries are expected, through tidal interaction, to have their rotation axes normal to their orbital plane, and in some eclipsing systems the spectrum can yield the direction of rotation. Close binaries, as well as spectroscopic binaries, can be modeled for stellar inclination to the line of sight implied from their orbital elements. Statistically, as in the study of star clusters, or in determining stellar spectral-type/rotational-velocity correlations, the average sine of the stellar inclination of the line of sight has been taken as $\pi/4$ (Allen 1976).

Stellar rotational velocities (V) determined from Doppler broadened spectral lines are dependent on the inclination i to the line of sight, so that only $V \sin i$ is measured.

In order to begin to find the space orientation of a star, one must first find a way to isolate the rotational-velocity component from the stellar inclination to the line of sight, as well as determine the clocklike, on-the-plane-of-the-sky orientation, which we will be identifying as the vector $\hat{\boldsymbol{n}}$. We have found that these components may be separable by looking at the stars in the Ca II H and K line emission associated with sunspot activity.

II. Ca II H AND K FLUX AND STELLAR ORIENTATION

Plage areas on the Sun, which cause Ca II H and K line emission in the usual broad absorption bands, have been shown to be associated with sunspot activity (e.g., Wilson 1968; Vaughan, Preston, and Wilson 1978; Wilson 1978; Vaughan and Preston 1980). Long-term variations, on the order of years, in the magnitudes of these emission lines have been used to follow late-type stellar sunspot or starspot cycles (Vaughan 1980; Wilson, Vaughan, and Mihalas 1981). Short-term variations, on the order of days, have been shown to yield the true rotation period (P) of the star (Vaughan 1981; Vaughan *et al.* 1981; Baliunas *et al.* 1983; Hartmann *et al.* 1983). The short-period variations are apparently due to the asymmetric distribution of the starspot regions on the western and eastern hemispheres alternately displayed toward the observer as the star rotates, thus causing the H and K emission to vary. Although other methods exist for the determination of the rotation periods of stars, this method is the most widely demonstrated at present.

Once the rotation period P is known, it can be combined with the stellar radius r, determinable by several methods (Fracassini, Pasinetti, and Manzolini 1981), to give the star's true rotational velocity: $V = 2\pi r/P$, assuming a spherical star, reasonable for slow, solar-type rotators. This velocity, divided into the projected Doppler velocity from spectral line broadening $V \sin i$, then gives the true stellar rotation axis inclination i to the line of sight. Table 1 lists preliminary values of the inclination to the line of sight for a number of stars whose rotation periods have been determined by the Ca II H and K emission method. Many more stellar rotation

[1] Present address: NASA/Ames Research Center, Space Sciences Division, M.S. 245-7, Moffett Field, CA 94035.

TABLE 1

DERIVED STELLAR INCLINATIONS TO THE LINE OF SIGHT

Star	$V \sin i$ (km s^{-1})	V (km s^{-1})	i
Sun	1.84	2	66°33′
HD 2454	8	8	90°
HD 22049	<3	4	$<49°$
HD 25998	22	23	73°
HD 26913	<6	7	$<59°$
HD 154417	5.5 ± 0.7	7	$52°^{+10°}_{-9°}$
HD 190406	3–5	4	49° – 90°
HD 206860	10.2 ± 1.1	11	$68°^{+22°}_{-12°}$

NOTE.—Radius values are from the mass-radius relationship for dwarf stars of Harris, Strand, and Worley 1963. $V \sin i$ values for HD 22049 are from Vogt, Penrod, and Soderblom 1983; for the Sun, HD 154417, and HD 206860, from Soderblom 1982; and for HD 2454, HD 25998, HD 26913, and HD 190406, from Kraft 1967. Ca II H and K periods as well as the above values are from Table 3 of Baliunas *et al.* 1983.

periods continue to be measured by this method, and advances in high-resolution spectroscopy may provide more accurate values of $V \sin i$.

The second component of axis tilt, the clocklike orientation $\hat{n}$, must rely on some latitudinal asymmetry, and again the Ca II H and K emission associated with sunspot activity can be of use. As observed on the Sun, sunspot activity is confined to ecliptic latitudes of $\pm 40°$ (see Allen 1976 and references therein). The H and K emission from plage areas associated with sunspot regions would thus be expected to be confined to a large equatorial belt, and a kind of solar "sash" or elliptical component does indeed characterize the Sun in this narrow wavelength region, as shown in Figure 1 (Plate 7). Measurements of solar-type stars in Ca II H and K emission at different angles should then give different radii, the longest being along the stellar equator. This would consequently give the stellar equator's clocklike orientation on the plane of the sky. This confinement of Ca II H and K emission to equatorial regions may apply to other than solar-type stars as well, but the effect of greater magnetic field strengths as well as the relationship between normal solar-type starspots and coronal hole–type phenomena, which generally form around the polar regions, must be better understood. (An example of the latter type of phenomenon can be found in Vogt and Penrod 1983.)

The first consideration in measuring this value might be to simply photograph the star simultaneously in visual and in H and K emission, then deconvolve the visual light point-spread function assuming a circular disk source. The H and K image similarly deconvolved should then be elliptical. However, with this approach the recorded stellar image, usually assumed to be Gaussian, would be at least two orders of magnitude larger than the original stellar size, and the deviations of the H and K image from circularity could very easily be hidden in the noise, so that a major and minor axis of an elliptical shape could not be accurately determined.

A direct measurement of the radii of the star in Ca II H and K flux must, therefore, be done. This requires a short review of the available direct stellar measuring techniques to determine the method most appropriate for use in the very limited light available in Ca II H and K emission.

III. TECHNIQUES FOR MEASURING STELLAR RADII

The major techniques for directly determining stellar radii are lunar occultations, intensity interferometry, Michelson interferometry, and speckle interferometry. The lunar occultation technique (first outlined in Williams 1939; and Evans 1955) can theoretically determine a star's finite angular extent by recording its disappearance time behind the Moon when it is occulted. In practice, one records a diffraction pattern due to the interception of the star's light by the cutting edge of the Moon (e.g., Barnes and Evans 1976). The diffraction pattern's measured deviation from a point source (smaller amplitudes) will give its finite extent. Occultation event times are of the order of milliseconds, and very fast photometers are required. The lunar occultation techniques would not appear to be practical at present for performing H and K stellar measurements, because of the very short event times and consequent lack of sufficient time to collect the photons required for a good determination. In addition, event times are scheduled by nature and not by the observer.

Intensity interferometry (Hanbury Brown *et al.* 1967; Hanbury Brown 1968) relies on the intrinsic statistical fluctuations in the sampled photon flux by measuring its arrival time at two different receivers and then integrating the differences over a large period of time. Integration times can be as long as 50 hours or more, and the technique is generally limited to stars of magnitude 2.0 or brighter. This technique would not, therefore, be sensitive enough to measure the star's radius in H and K flux alone. The authors of this method have suggested, however, that it could be used to measure oblateness of rapidly rotating early-type stars of sufficient brightness, a problem not unlike the one being investigated in this paper.

Michelson interferometry, as first performed by Michelson and Pease (1921), used one telescope with four smaller mirrors, two located at opposite ends of a 20 foot (6 m) beam attached to the observing-cage end of the telescope. These two directed light from a star inward toward the other two small mirrors, which, in turn, directed it down to the telescope mirror, where the beams could interfere with each other. By varying the separation of the two mirrors and recording the separation at which the interference fringes disappeared, the angular extent of the star could be measured. The technique, however, would seem to be limited by a lack of observers practiced in the art of recognizing when the fringes indeed disappear, as well as being constrained by atmospheric turbulence. The 20 foot baseline is one-dimensional, and would appear to be approaching a visual ground-based limit for such a

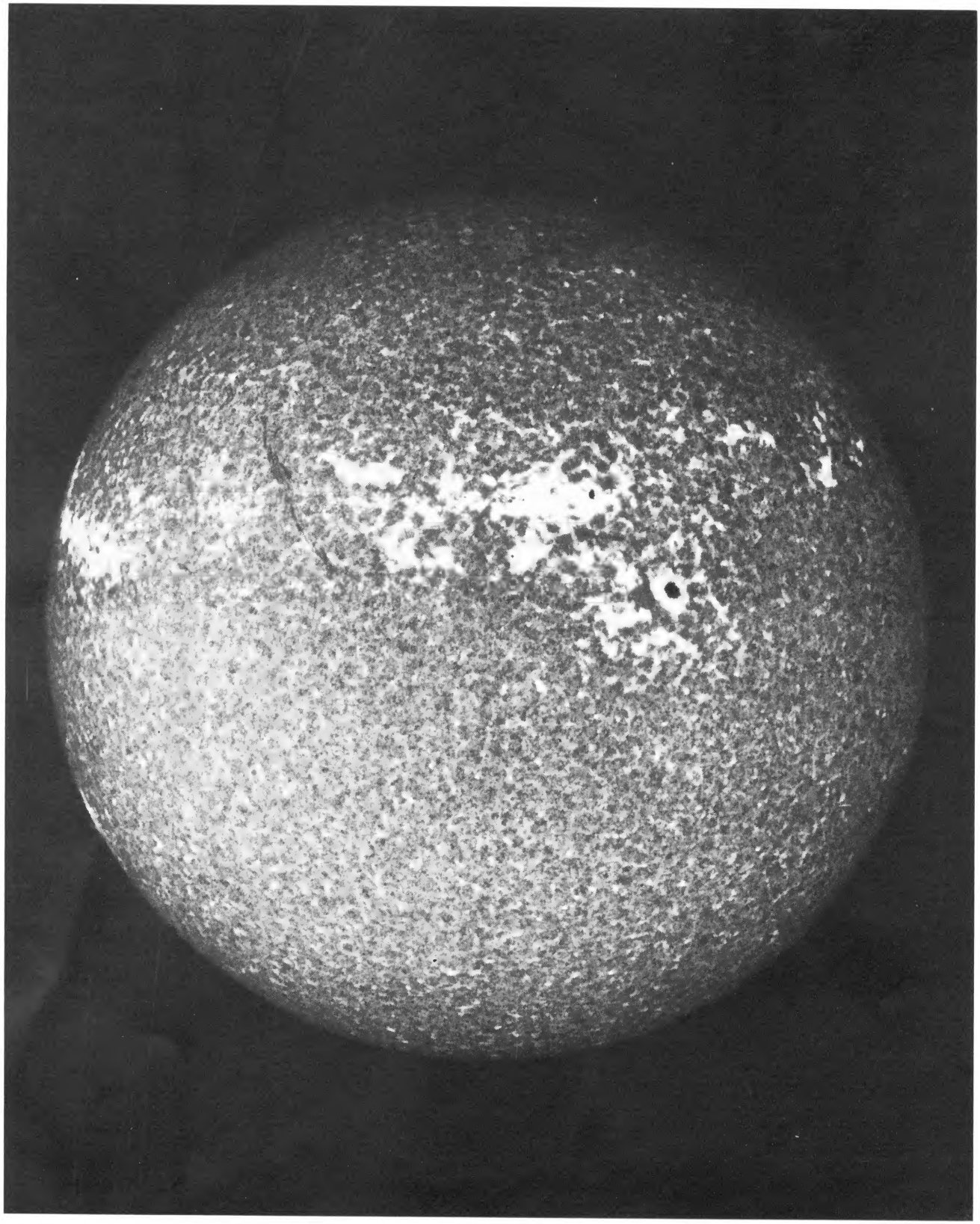

FIG. 1.—Picture of the Sun taken in Ca II K emission (3933.664 Å) showing the equatorial "sash" indicative of the Sun in this wavelength. (Photo courtesy of the Mount Wilson and Las Campanas Observatories, Carnegie Institution of Washington.)

DOYLE *et al.* (*see* page 308)

device without the interference fringes becoming largely imperceptible. However, such an interferometer in orbit would not share such baseline limitations and would be of great value in determining stellar radii. Some modifications of their concept show promise as well (e.g., Breckinridge 1972; Roddier and Roddier 1982).

Speckle interferometry (Labeyrie 1970; Gezari, Labeyrie, and Stachnik 1972; Labeyrie *et al.* 1974), by far the most sensitive of the Earth-based techniques, has presently been performed on stars down to 16th magnitude. Extensions of the technique have included precise star mapping (Liu and Lohmann 1973), application to infrared wavelengths in one dimension (Howell, McCarthy, and Low 1981), and image reconstruction (e.g., Nisenson and Stachnik 1979). Current work includes a differential speckle interferometry concept using narrow (less than 1 Å) bandpass filters (Beckers and Hege 1982), which may improve $V \sin i$ values of stellar rotation significantly.

Speckle interferometry generally utilizes a single telescope to record a quick-exposure speckle pattern of photons which are the image of, for example here, a close binary system. The stars are theoretically resolvable but are convolved by atmospheric turbulent cells and the distribution pattern of the finite-aperture telescope. The assumption of theoretical resolution is usually made so that the specks that make up the speckle pattern do not further complicate the image by being as small as the Airy disk. Although the convoluted images of the two stars are superposed, the basic offset of each pattern (spatial frequency of separation of the two stars) remains. By taking the Fourier transform of the total speckle pattern, this frequency become evident, and the angular separation of the two stars is determined. Similarly, for single stars, the characteristic frequency would be the integrated finite extent of the star's disk. Exposure times generally need to be less than 0.1 s to "freeze" the atmospheric cells producing the speckle pattern. By taking the Fourier transform of the speckle pattern, the spatial frequencies invert and small spatial frequencies due to the finite extent of the star become large interference rings, while the large convolution due to the atmospheric turbulent cells become specklike in the Fourier transform space image. The Fourier transformed speckle images can thus be superposed to build up the photon signal-to-noise ratio. This method, with slight modifications, will now be applied to the problem of measuring a star's elliptical axes in Ca II H and K line emission.

IV. Ca II H AND K EMISSION SPECKLE INTERFEROMETRY

In this application, we will want to measure the axis direction on the plane of the sky of the elliptical component of a star in Ca II H and K emission. Since the intensity distribution curve of the Fourier transformed speckle image will flatten in higher orders as the source deviates from a point source, the ability to measure differences in Fourier transformed photon counts of these higher order maxima and minima is what is statistically required. The expected intensity distribution for an elliptical source in Fourier transform space would thus have elliptical intensity rings, but rotated 90° from the actual source orientation, as will be shown. The orientation of the semimajor and semiminor axes of this image and the accuracy with which they can be determined will be derived. Since photon flux in Ca II H and K emission is extremely limited, we will want to calculate the photon statistical limits for the resolution of these small object parameters (major and minor axes of a stellar image) through atmospheric turbulence.

We start by defining a digital-image approach to the reduction and processing of the speckle pattern. The images of the speckle pattern will thus be made up of many individual picture elements (pixels). We define $G(\boldsymbol{y}_j)$ to be the number of photons in one speck of the speckle image (its intensity or DN number). Each speck j is labeled by its position vector $\boldsymbol{y}_j$. We also assume that the angular size of the object (star) is much smaller than the angle subtended by the turbulent cell responsible for the proliferation of speckle images—certainly supported by observations.

A complete speckle image will be made up of many individual specks, all of an object assumed to be within the theoretical resolution limit of the telescope, so that, as mentioned before, they are not as small as the Airy disk.

Next, the resolution limit of the digital image is chosen to be of sufficient size that each speck in the speckle image is spread over N_I pixels. Consider first the one-dimensional problem. The total speckle image then consists of a data set that may be represented by

$$\{G_j(x_n + y_j)\}$$

where y_j is the vector center location of the speck, and x_n is the pixel ordinate within an individual speck, so that

$$x_n = n\Delta ,$$

where Δ is the length of a pixel (n of them constitute a speck length) and

$$\frac{-N_I}{2} \leq n \leq \frac{N_I}{2} ,$$

N_I as defined being the length of an individual speck.

In processing a speckle image, either with a laser or digitally, the Fourier transform of the image is taken in order to separate the low-frequency components of the atmosphere from the high-frequency components of the stellar image.

Let us consider, then, the Fourier transform, $\{\tilde{G}\}$, of the speckle image $\{G_j(x_n + y_j)\}$. Letting k be the wavenumber $(2\pi/\lambda)$, we have for the real component

$$\tilde{G}(k) = \sum_j \sum_n \cos k(x_n + y_j) G_j(x_n + y_j) = \sum_j \sum_n G_j(x_n + y_j) \cos (nk\Delta + ky_j) , \quad (1)$$

where

$$\sum_j \sum_n G_j(x_n + y_j) = \sum_j \sum_n (G_0 + \delta G_{jn}) , \quad (2)$$

the δG_{jn} being the deviations from the mean intensity values recorded per pixel and G_0 the mean number of photons per pixel, or

$$G_0 = \frac{N}{N_I N_s}, \tag{3}$$

where N is the total number of photons in the speckle image, N_I is the number of pixels per speck, as before, and N_s is the number of specks per speckle image. Substituting equation (2) in equation (1), we obtain

$$\tilde{G}(k) = G_0 \sum_j \sum_n \cos(nk\Delta + ky_j) + \sum_j \sum_n \delta G_{jn} \cos(nk\Delta + ky_j). \tag{4}$$

From the first term in equation (4), we can write

$$\sum_n \cos(nk\Delta + ky_j) = \tfrac{1}{2} \sum_n (e^{i(ky_j + nk\Delta)} + e^{-i(ky_j + nk\Delta)}) = \tfrac{1}{2}\left(e^{iky_j} \sum_{-N_I/2}^{N_I/2} e^{ink\Delta} + e^{-iky_j} \sum_{-N_I/2}^{N_I/2} e^{ink\Delta} \right). \tag{5}$$

Using the series sum identity, $\sum_n (1 + z + z^2 + \cdots + z^n) = (1 - z^{n+1})/(1 - z)$, the summation terms can be written

$$\sum_{-N_I/2}^{N_I/2} e^{ink\Delta} = e^{(-iN_I/2)k\Delta} \frac{1 - e^{i(N_I+1)k\Delta}}{1 - e^{ik}} = \frac{\sin[(1/2)(N_I + 1)k\Delta]}{\sin(1/2)k\Delta}. \tag{6}$$

We notice now, that the terms in $\sum_n \sum_j \delta G_{jn} \cos(nk\Delta + ky_j)$ are all uncorrelated. Furthermore, the δG_{jn} are the results of counting errors, which, according to Poisson statistics, will have characteristic magnitude $G_0^{1/2}$. The uncorrelated sum can be thought of as a random walk with a total of $N_I N_s$ steps having a characteristic net length of $(N_I N_s)^{1/2}$. Therefore, the net uncertainty in the Fourier transformed quantities $\tilde{G}(k)$ is just $N^{1/2}$.

$$\tilde{G}(k) = \frac{N}{N_I N_s} \sum_j \cos ky_j \frac{\sin[(1/2)(N_I + 1)k\Delta]}{\sin(1/2)k\Delta} \pm N^{1/2}. \tag{7}$$

By a similar line of reasoning, the sum $\sum_j \cos ky_j$ involves uncorrelated terms for sufficiently large k, and the characteristic total magnitude is $N_s^{1/2}$. Thus,

$$\tilde{G}(k) \approx \frac{N}{N_I N_s^{1/2}} \frac{\sin[(1/2)(N_I + 1)k\Delta]}{\sin(1/2)k\Delta} \pm N^{1/2}. \tag{8}$$

Equation (8) describes the inversion of spatial scales which is the key to understanding the utility of Fourier transform space for mitigating the effects of turbulence (Fig. 2). The existence of many individual specks contributes to the graininess of the Fourier image; a single speck defines large-scale envelope structures. The appropriate pixel spacing in k-space (Fourier transform space), Δk, is related to the initial pixel image, Δx, by the relation

$$\Delta k \approx \frac{2\pi}{N_p \Delta x}, \tag{9}$$

where N_p is the total number of pixels.

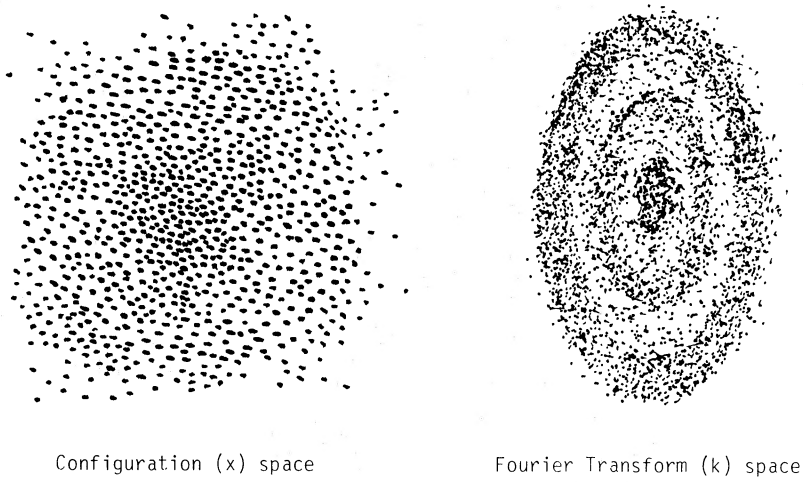

FIG. 2.—Simplified diagram of stellar Ca II H and K speckle image transformation to Fourier transform space

So far we have been concerned with one-dimensional distributions. Since we are actually interested in two-dimensional images, we consider briefly the speckle image of a circular disk. Defining

$$\tilde{G}(k) \equiv \sum_j \sum_n e^{i\boldsymbol{k}\cdot(\boldsymbol{x}_n+\boldsymbol{y}_n)} G_j(\boldsymbol{x}_n+\boldsymbol{y}_j)\,, \tag{10}$$

where $\boldsymbol{x}_n$ and $\boldsymbol{y}_n$ now denote *two-dimensional* pixel and speck coordinates, and introducing polar coordinates within each individual speck, we obtain

$$\tilde{G}(k) = \frac{1}{\Delta^2}\sum_j \frac{N}{N_I N_s}\int_0^a\int_0^{2\pi} e^{i(\boldsymbol{k}\cdot\boldsymbol{y}_j + kr\cos\theta)} r dr d\theta = \frac{2\pi a}{k\Delta^2}\frac{N}{N_I N_s} J_1(ka)\sum_j e^{i\boldsymbol{k}\cdot\boldsymbol{y}_j}\,, \tag{11}$$

or

$$\tilde{G}(\boldsymbol{k}) \approx \frac{2\pi a}{k\Delta^2}\frac{N}{N_I N_s^{1/2}} J_1(ka) \pm N^{1/2}\,, \tag{12}$$

where a is the characteristic radius, and J_1 is the ordinary Bessel function of order 1. The argument leading to the uncertainty term $N^{1/2}$ in equation (12) follows exactly the one-dimensional case.

Since we are actually interested in finding the (Fourier transformed) principal axes of an elliptical distribution, we shall now define a measure of oblateness. If

$$H(\hat{\boldsymbol{n}}) \equiv \sum_i \sum_j [(\boldsymbol{K}_{ij} - \langle \boldsymbol{K}\rangle)\cdot\hat{\boldsymbol{n}}]^2 \tilde{G}_{ij}\,, \tag{13}$$

then it can be shown that H has near-stationary values when the unit vector $\hat{\boldsymbol{n}}$ points in a small interval of directions near the oblateness axes. The quantity $\langle \boldsymbol{K}\rangle$ is just the centroid of the total distribution:

$$\langle \boldsymbol{K}\rangle \equiv \frac{\sum_i \sum_j K_{ij} G_{ij}}{\sum_i \sum_j \tilde{G}_{ij}}\,, \tag{14}$$

where the vectors $\boldsymbol{K}_{ij}$ define the locations of the pixel centers in the Fourier transform domain. It is convenient to define the vector derivative quantity $\partial H/\partial\hat{\boldsymbol{n}}$, which is related to the gradient:

$$\frac{\partial H}{\partial \hat{\boldsymbol{n}}} = \lim_{|\hat{\boldsymbol{n}}'-\hat{\boldsymbol{n}}|\to 0} \frac{H(\hat{\boldsymbol{n}}') - H(\hat{\boldsymbol{n}})}{|\hat{\boldsymbol{n}}' - \hat{\boldsymbol{n}}|^2}(\hat{\boldsymbol{n}}' - \hat{\boldsymbol{n}})\,. \tag{15}$$

In terms of this quantity, the defining equation for the oblateness axes is given by

$$\hat{\boldsymbol{n}}_1 \times \frac{\partial H}{\partial \hat{\boldsymbol{n}}_1} = 0\,, \tag{16}$$

i.e., near the direction defined by the unit vector $\hat{\boldsymbol{n}}_1$ the oblateness function H is stationary. Equation (16) reduces to the form

$$\sum_i \sum_j (\boldsymbol{\Delta}_{ij}\cdot\hat{\boldsymbol{n}})\hat{\boldsymbol{n}} \times \boldsymbol{\Delta}_{ij}\tilde{G}_{ij} = 0\,, \tag{17}$$

where

$$\boldsymbol{\Delta}_{ij} \equiv \boldsymbol{K}_{ij} - \langle \boldsymbol{K}\rangle\,. \tag{18}$$

Now the precision with which the true value of the oblateness axes, $\hat{\boldsymbol{n}}$, can be determined evidently depends upon the statistics of the quantities $\tilde{G}_{ij}$. A first-order expansion of equation (17) in terms of error quantities is given by

$$\sum_i \sum_j [(\boldsymbol{\Delta}_{ij}\cdot\delta\hat{\boldsymbol{n}})\hat{\boldsymbol{n}} \times \boldsymbol{\Delta}_{ij}\tilde{G}_{ij} + (\boldsymbol{\Delta}_{ij}\cdot\hat{\boldsymbol{n}})\delta\hat{\boldsymbol{n}} \times \boldsymbol{\Delta}_{ij}\tilde{G}_{ij} + (\boldsymbol{\Delta}_{ij}\cdot\hat{\boldsymbol{n}})\hat{\boldsymbol{n}} \times \boldsymbol{\Delta}_{ij}\delta\tilde{G}_{ij}] = 0\,, \tag{19}$$

where $\delta\hat{\boldsymbol{n}}$ is perpendicular to $\hat{\boldsymbol{n}}$ at the stationary point. Now it is easy to show, as a vector identity,

$$(\boldsymbol{r}\cdot\delta\hat{\boldsymbol{n}})\hat{\boldsymbol{n}} \times \boldsymbol{r} + (\boldsymbol{r}\cdot\hat{\boldsymbol{n}})\delta\hat{\boldsymbol{n}} \times \boldsymbol{r} = \hat{\boldsymbol{k}} r^2 |\,\delta n|\,. \tag{20}$$

Combining equations (19) and (20), we obtain the result

$$|\,\delta\hat{\boldsymbol{n}}| = \frac{|\sum_i \sum_j (\boldsymbol{\Delta}_{ij}\cdot\hat{\boldsymbol{n}})\hat{\boldsymbol{k}}\cdot\hat{\boldsymbol{n}} \times \boldsymbol{\Delta}_{ij}\delta\tilde{G}_{ij}|}{\sum_i \sum_j |\boldsymbol{\Delta}_{ij}|^2 \tilde{G}_{ij}}\,. \tag{21}$$

It can be concluded from the form of equation (21) that oblate distributions of large eccentricity will have small values of $|\,\delta\hat{\boldsymbol{n}}|$. This results from the fact that a circular distribution minimizes the denominator. In order to establish a useful bound, we shall, therefore, assume a circular form, which considerably simplifies evaluation. We note, however, that for a true circular distribution, the function

$H(\hat{\boldsymbol{n}})$ is independent of direction, $\hat{\boldsymbol{n}}$, and there is no favored axis of oblateness. Consider now

$$\sum_i \sum_j |\Delta_{ij}|^2 \tilde{G}_{ij} \approx \frac{1}{(\Delta k)^2} \int k^2 \tilde{G}_0 \, d^2\boldsymbol{k} = \frac{2\pi}{(\Delta k)^2} \int_0^{k_{\max}} \tilde{G}_0(k) k^3 dk$$

$$= \left(\frac{2\pi}{\Delta k \Delta x}\right)^2 a \frac{N}{N_I N_s^{1/2}} \int_0^{k_{\max}} J_1(ka) k^2 dk$$

$$= \left(\frac{2\pi}{\Delta k \Delta x}\right)^2 \frac{N}{N_I N_s^{1/2}} k_{\max}^2 J_2(k_{\max} a) , \tag{22}$$

where we have used the Fourier transformed circular distribution described by equation (12). The numerator in equation (21) can be evaluated approximately as follows:

$$\left| \sum_i \sum_j (\Delta_{ij} \cdot \hat{\boldsymbol{n}}) \hat{\boldsymbol{k}} \cdot (\hat{\boldsymbol{n}} \times \Delta_{ij}) \delta \tilde{G}_{ij} \right| \approx \tfrac{1}{2} k_{\max}^2 (N N_p)^{1/2} , \tag{23}$$

where N_p is the total number of pixels in either configuration or Fourier transform space. We have used the result here that $\delta \tilde{G}_{ij} = N^{1/2}$ and the fact that the combination $\Delta k \Delta x$ can be eliminated from equation (22) using the relation

$$(\Delta k \Delta x)^2 = \frac{(2\pi)^2}{N_p} , \tag{24}$$

which defines the connection between the two-dimensional configuration and Fourier transform space increments in terms of the total number of independent discrete elements. Combining equations (21)–(24), we obtain finally

$$|\delta \hat{\boldsymbol{n}}| \approx \frac{1}{2 J_2(k_{\max} a)} N_I \left(\frac{N_s}{N N_p}\right)^{1/2} \approx N_I \left(\frac{N_s}{N N_p}\right)^{1/2} . \tag{25}$$

Recall that N_I is the number of pixels in a configuration space speck, N is the total number of photons, N_p is the total number of configuration or Fourier domain pixels, and N_s is the number of specks.

Equation (25) characterizes the quantum statistical limits of precision attainable in determining the elliptical axes of an oblate stellar object imaged on the plane of the sky, as seen through the turbulent atmosphere with a sufficiently large (i.e., image-resolving) telescope. It states, in effect, that once a telescope aperture is sufficiently large to resolve the stellar angular width, further increases in aperture size will not improve the oblateness axis resolution, since the total number of specks and the overall photon count will increase proportionately, thereby producing simple cancellation according to equation (25). Furthermore, overdefinition of the stellar images by allowing too many pixels per speck is also undesirable, since the distribution of a limited number of photons over too many sampling cells (pixels) leads to a statistical degradation in determining relatively simple features of the distribution, such as oblateness axes. On the other hand, accurate definition of an oblate axis $\hat{\boldsymbol{n}}$ requires that the image be not too crude.

Perhaps the best strategy for determining the stellar oblateness axes with precision is to simply take many separate short-time (10^{-3}–10^{-2} s) exposures. Note that multiply exposing the same piece of film produces no net improvement in resolution, since N_s and N increase proportionately, thereby leading to a net cancellation in equation (25). If N_e is the number of exposures from which the oblateness axes are determined, then it can be expected that the error in $\delta \hat{\boldsymbol{n}}$ will be further reduced, and we obtain the relation

$$|\delta \hat{\boldsymbol{n}}| \approx N_I \left(\frac{N_s}{N N_p N_e}\right)^{1/2} . \tag{26}$$

We will now review the inaccuracies in the determination of the inclination to the line-of-sight component as a prelude to applying the above formula for the determination of the uncertainties in the plane-of-the-sky angle.

V. PRECISION IN i AND $\hat{\boldsymbol{n}}$

The determined inclination to the line of sight, being dependent on the sine function, becomes increasingly sensitive as values approach 90°, and faster stellar rotations, unfortunately uncharacteristic in solar-type stars, would provide greater accuracy. As an example, for a star with a measured $V \sin i$ of 5 km s^{-1} with an uncertainty of 1 km s^{-1}, and a true rotational velocity of 7 km s^{-1}, the determination of i would be 45^{+14}_{-10} degrees. For an uncertainty of 1 km s^{-1} in the determination of the true velocity alone the inclination would be 45^{+11}_{-6} degrees. Recent developments in high-resolution spectroscopy and other techniques (e.g., Campbell 1983; Beckers and Hege 1982) can allow determinations of $V \sin i$ to sub–km s^{-1} values, which could allow a determination of i to better than 10°.

Uncertainties in the true rotational velocity determination arise from errors in both the Ca II H and K period determination as well as the stellar radius value used. For the stars listed in Table 1, the error in the determination of the Ca II H and K rotational period is of the order of 2%, which for a "known" radius translates to an inaccuracy in the true velocity of around 0.1 km s^{-1}. Further data being taken will reduce this still further.

The stellar radius itself can be found by a variety of direct and indirect methods (see Fracassini, Pasinetti, and Manzolini 1981 and references therein). Stellar radius will vary with wavelength as well. In addition, one would ideally want a value of the stellar radius at the region in the stellar atmosphere responsible for the formation of the spectral lines used in the determination of the ($V \sin i$) rotational broadening, although this is not usually specifiable. For the case of α Orionis (Betelgeuse), radius measurements in one

wavelength are given as accurate to within 1% (Lynds, Worden, and Harvey 1976), although the limb-darkening model will make a significant difference. Such an error in the determination of the radius alone translates to an uncertainty in the value of the "true" rotational velocity of about 0.1 km s^{-1}. It is therefore estimated that, with techniques presently available, the inclination to the line of sight of certain nearby stars could be determined to within 10° or better.

One important ambiguity in the interpretation of the data should also be pointed out. Although i specifies the inclination to the line of sight, it does not specify whether it is the northern pole (counterclockwise rotation) or the southern pole (clockwise rotation) of the star that is tilted toward the observer. Thus, there will be two possible values for the pointing direction of the pole along the line of sight, that is, two points, at $90° \pm i$. This would not, however, affect any of the immediate applications (to be discussed in § VI).

One would also expect the Ca II H and K emission available to vary not just with intrinsic starspot cycles but with inclination (from star to star) to the line of sight. Higher values of inclination would produce a more face-on view of the H and K emission and, by this effect, higher amplitudes in their variations. Pole-on views might be expected to diminish this emission greatly (in addition to showing no variability). Since the semiminor axis of the elliptical distribution of the star in H and K emission would foreshorten as the sine of the inclination to the line of sight, one could mention that the ratio of the semiminor to the semimajor axis might be an indicator of the actual inclination to the line of sight. However, aside from the decrease in the H and K emission available, measurement of the semiminor axis could be complicated by the fact that its angular extent is below the theoretical resolution limit. Also, the H and K emission region on the star is probably not uniform enough to measure an axis ratio dependably in this way. (One must remember that while the nonuniformities in the distribution of the Ca II H and K emission areas cause the rotational variations that allow the determination of the inclination to the line-of-sight component, it is these same nonuniformities that are the major sources of error in the determination of the major axis of the elliptically modeled "sash" region that gives the clocklike angle component on the plane of the sky.) In addition, a second-order effect would become important.

Because of the wide distribution of the Ca II H and K emission plage areas expected on solar-type stars (middle stellar latitudes), the effect of sphericity of the star is negligible to first order, and we can indeed determine an elliptical fit for the distribution of the H and K emission. The lines of equilatitude on the star are actually curves, and this "smile" or "frown" orientation, while theoretically being able to remove the dual axis ambiguity mentioned earlier, could also not be expected to be well enough defined to make any such determination possible.

We will now want to calculate a numerical estimate of stellar brightness requirements for determination of the axis ($\hat{\boldsymbol{n}}$) orientation or the plane of the sky.

The number of photons available for the axis-orientation measurement of an Mth magnitude star can be expressed by the equation

$$\frac{N}{N_s} = \frac{\Delta v}{v} \frac{QSA\tau}{E_p N_s} 10^{-0.4(M+26)}, \tag{27}$$

where the Sun's apparent magnitude is taken as -26, $\Delta v/v$ is the fractional line width of the filtered Ca II H and K light, Q is the quantum efficiency, S is the solar constant, A is the aperture area of the telescope, τ is the exposure time, and E_p is the photon energy. Equations (26) and (27) can be combined to yield a threshold brightness requirement:

$$M = 2.5 \log_{10} \left[\left(\frac{\delta n}{N_I} \right)^2 N_p N_e \frac{\Delta v}{v} \frac{QSA\tau}{N_s E_p} \right] - 26 . \tag{28}$$

As a representative set of parameters, let us take $Q = 0.2$, $S = 10^3$ W m^{-2}, $\tau = 10^{-3}$ s, $A/N_s = 2.5 \times 10^{-4}$ m^2, $E_p = 2.5$ eV, $\Delta v/v = 2 \times 10^{-4}$, $N_p = 10^6$, $N_e = 10^2$, $N_I = 10^2$, and $\delta n = 0.1$ (about 6°).

We obtain a threshold magnitude of $M = 5$. Of course, there is a great deal of uncertainty in what constitutes a reasonable set of parameters for an axis-orientation measurement. The set we have chosen is rather conservative. In particular, the number of pixels is determined by the grain size if the image is recorded on film, and N_p could easily exceed the chosen value by one or two orders of magnitude. In addition, the number of exposures could be manageably increased by an order of magnitude. We conclude that these kinds of techniques can plausibly be extended substantially beyond this limit.

VI. APPLICATIONS AND CONCLUSIONS

There are many important applications for the determined space orientations of stars. The determination of stellar orientations in binary and multiple star systems as well as in clusters could have important consequences for theories on the formation and evolution of star systems. For example, determining the distribution of spin axes in stellar clusters would provide insight into angular momentum distribution in primordial clouds from which the stars formed and thus into the compression phenomenon which initiates gravitational collapse.

Incidentally, timing any differences in the ingress and egress as well as the duration of an eclipse in an eclipsing binary system in visual and in Ca II H and K emission could provide information with which the stellar pole orientations could be compared with their orbital plane. This could be compared with an independent measurement from Ca II H and K speckle interferometry of the orientation component $\hat{\boldsymbol{n}}$ on the plane of the sky.

Of more immediate utility, however, would be the application of the determination of stellar space orientations to the search for extrasolar planetary systems. A number of important applications exist. As our solar system indicates, supported by both theories and preliminary observations, planetary bodies are expected to form in orbits in or near the star's equatorial plane (e.g., Isaacman and Sagan 1977). Determining the star's space orientation, then, would give the expected planetary plane.

Two methods proposed for finding extrasolar planets involve wobbling of the star due to the gravitational influence of the unseen (planetary) companion. A known inclination to the line of sight immediately tells the observer in which direction the star would be expected to wobble, and therefore which detection method to use: radial velocity variations or proper-motion wobbles (see Black 1980 for a review).

Another, the photometric method (Borucki and Summers 1983), would measure the luminosity drop in a star's brightness due to the transit of a planetary body across the face of the star. Knowing the inclination of stars would allow differentiation of the stars inclined favorably for such a transit to occur in our line of sight.

Determining the complete space orientation of a star could allow intrinsic stellar pulsation components to be separated from an external secondary body's gravitational influence, and thereby the expected location of the secondary body in relation to the star could be formulated. Knowing the expected planetary orbital plane in conjunction with the gravitational influence of the external perturbing body thus highly constrains and thereby greatly enhances the possibility of detecting extrasolar planetary systems.

We conclude, then, that with this method the space orientation of certain stars may be determinable to better than 10° for both components, thereby adding a new and very useful primary parameter to the known characteristics of stars.

We would first of all like to thank Gary A. Fouts of Mount Wilson and Las Campanas Observatories, without whose insights, enthusiasm, and encouragement this project would probably not have been started. Thanks also go to Sallie Baliunas of the Center for Astrophysics, Cambridge, Massachusetts, for preprints of the most recent Ca II H and K observations, and to Dave Pieri of Jet Propulsion Laboratory for his unfailing support. Finally, we would like to thank Dr. Myron Smith for his very helpful refereeing of the paper and Dr. Helmut Abt for information on stellar inclinations determined for Ap stars. Figure 1 was provided by courtesy of Mount Wilson and Las Campanas Observatories.

REFERENCES

Abt, H. A. 1972, *Ap. J.*, **175**, 779.
Allen, C. W. 1976, *Astrophysical Quantities* (3d ed.; London: Athlone), pp. 210, 183.
Baliunas, S. L., *et al.* 1983, *Ap. J.*, **275**, 752.
Barnes, T. G., and Evans, D. S. 1976, *M.N.R.A.S.*, **174**, 489.
Beckers, J. M., and Hege, E. K. 1982, in *IAU Colloquium 67, Instrumentation for Astronomy with Large Optical Telescopes*, ed. C. M. Humphries (Dordrecht: Reidel), p. 199.
Black, D. C. 1980, *Space Sci. Rev.*, **25**, 35.
Borucki, W. J., and Summers, A. L. 1983, preprint.
Breckinridge, J. B. 1972, *Appl. Optics*, **11**, 2996.
Campbell, B. 1983, *Pub. A.S.P.*, **95**, 577.
Doyle, L. R., Wilcox, T. J., and Lorre, J. J. 1983, *Pub. A.S.P.*, **95**, 588.
Evans, D. S. 1955, *M.N.R.A.S.*, **115**, 467.
Fracassini, M., Pasinetti, L. E., and Manzolini, F. 1981, *Astr. Ap. Suppl.*, **45**, 145.
Gezari, D. Y., Labeyrie, A., and Stachnik, R. V. 1972, *Ap. J. (Letters)*, **173**, L1.
Hanbury Brown, R. 1968, *Ann. Rev. Astr. Ap.*, **6**, 13.
Hanbury Brown, R., Davis, J., Allen, L. R., and Rome, J. M. 1967, *M.N.R.A.S.*, **137**, 393.
Harris, D. L., Strand, K. Aa., and Worley, C. E. 1963, in *Stars and Stellar Systems*, Vol. **3**, *Basic Astronomical Data*, ed. K. Aa. Strand (Chicago: University of Chicago Press), p. 273.
Hartmann, L., Baliunas, S. L., Noyes, R. W., and Duncan, D. K. 1983, Center for Astrophysics, Preprint No. 1818.
Howell, R. R., McCarthy, D. W., and Low, F. J. 1981, *Ap. J. (Letters)*, **251**, L21.
Isaacman, R., and Sagan, C. 1977, *Icarus*, **31**, 510.
Kraft, R. P. 1967, *Ap. J.*, **150**, 551.
Labeyrie, A. 1970, *Astr. Ap.*, **6**, 85.
Labeyrie, A., Bonneau, D., Stachnik, R. V., and Gezari, D. Y. 1974, *Ap. J. (Letters)*, **194**, L147.
Liu, Y. C. C., and Lohmann, A. W. 1973, *Optics Comm.*, **8**, 372.
Lynds, C. R., Worden, S. P., and Harvey, J. W. 1976, *Ap. J.*, **207**, 174.
Michelson, A. A., and Pease, F. G. 1921, *Ap. J.*, **53**, 249.
Nisenson, P., and Stachnik, R. 1979, in *IAU Colloquium 50, High Angular Resolution Stellar Interferometry*, ed. J. Davis and W. J. Tango (Sydney: University of Sydney), p. 34.
Roddier, F., and Roddier, C. 1982, in *IAU Colloquium 67, Instrumentation for Astronomy with Large Optical Telescopes*, ed. C. M. Humphries (Dordrecht: Reidel), p. 207.
Soderblom, D. R. 1982, *Ap. J.*, **263**, 239.
Vaughan, A. H. 1980, *Pub. A.S.P.*, **92**, 392.
———. 1981, *Annual Report of the Mount Wilson and Las Campanas Observatories, 1980–1981*, p. 599.
Vaughan, A. H., Baliunas, S. L., Middelkoop, F., Hartmann, L., Mihalas, D., Noyes, R. W., and Preston, G. W. 1981, *Ap. J.*, **250**, 276.
Vaughan, A. H., and Preston, G. W. 1980, *Pub. A.S.P.*, **92**, 385.
Vaughan, A. H., Preston, G. W., and Wilson, O. C. 1978, *Pub. A.S.P.*, **90**, 267.
Vogt, S. S., and Penrod, G. D. 1983, *Pub. A.S.P.*, **95**, 565.
Vogt, S. S., Penrod, G. D., and Soderblom, D. R. 1983, *Ap. J.*, **269**, 250.
Williams, J. D. 1939, *Ap. J.*, **89**, 467.
Wilson, O. C. 1968, *Ap. J.*, **153**, 221.
———. 1978, *Ap. J.*, **226**, 379.
Wilson, O. C., Vaughan, A. H., and Mihalas, D. 1981, *Sci. Am.*, **244**, 104.

LAURANCE R. DOYLE: 3543 Santa Carlotta, La Crescenta, CA 91214

JEAN J. LORRE and THOMAS J. WILCOX: Research and Development Laboratories, 19450 Pacific Gateway Drive, Torrance, CA 90502